nature communications

Article

https://doi.org/10.1038/s41467-025-66537-7

Controlled microphase separation and strain programming in hydrogel fibers toward biomimetic architectures and properties

Received: 6 June 2025

Accepted: 10 November 2025

Published online: 29 November 2025

Check for updates

Jian Yang[1,5], Congcong Chen[1,5], Yu Wang[1], Lijun Yang[1], Xinglong Pan[2], Ghim Wei Ho[2], Qing Zhang[3], Shichao Niu[4] & Xiao-Qiao Wang[1]

In contrast to conventional high-strength, high-modulus fibers, spider silk uniquely combines high toughness, strength and diverse functionalities, enabling spiders to thrive in natural environments. However, replicating the sophisticated architecture and properties of spider silk through synthetic approaches, particularly via scalable fiber manufacturing processes, remains a formidable challenge. Herein, we report the tailored fabrication of spider silk-like structures in sodium polyacrylate and polyacrylamide (PANa-PAM) composite polymer hydrogel fibers via wet-spinning. The antisolvent-induced phase separation process modulates composite polymer microphase, yielding nascent PANa-PAM fibers abundant in hydrogen-bonded nanoclusters. Subsequent post-drawing for strain programming facilitates uniaxial polymer alignment and controlled crystallization. The optimized fiber comprises aligned microfibrils, polymer-rich rigid nanoclusters surrounded by polymer-loose regions, and β-sheet-like crystallites, closely mimicking the hierarchical architecture of natural spider silk. As a result, the composite fiber achieves a comprehensive set of spider silk-like properties and functionalities, including a toughness of 118.7 MJ m^{-3}, a tensile strength of 172.3 MPa, 50% elastic strain recovery, 96% damping efficiency, 60% supercontraction, and moisture sensitivity. This bioinspired wet-spinning of composite polymer hydrogels offers a pathway to replicate biological fiber structures and attributes, enabling the production of high-performance and intelligent fibers for wearable technologies.

Modern fiber technologies increasingly demand materials with exceptional mechanical properties, multifunctionality, and intelligence, advancing emerging applications toward impact protection gear[1], wearable electronics[2], and artificial muscles[3]. Commercial high-performance fibers are renowned for their high strength and modulus, achieved through highly aligned molecular chains and crystalline structures. However, their lack of ductile components results in limited extensibility and, consequently, insufficient toughness, restricting their ability to absorb high-impact energy in protective applications[4]. Among these, ultrahigh-molecular-weight polyethylene (UHMWPE)

[1]National Engineering Laboratory for Modern Silk, College of Textile and Clothing Engineering, Soochow University, Suzhou 215123 Jiangsu, P. R. China. [2]Department of Electrical and Computer Engineering, National University of Singapore 4 Engineering Drive 3, Singapore 117583, Singapore. [3]Vacuum Interconnected Nanotech Workstation, Suzhou Institute of Nano-Tech and Nano-Bionics, Chinese Academy of Sciences, Suzhou 215123 Jiangsu, P. R. China. [4]Key Laboratory of Bionic Engineering (Ministry of Education), Jilin University, Changchun 103022 Jilin, P. R. China. [5]These authors contributed equally: Jian Yang, Congcong Chen e-mail: xqwang@suda.edu.cn

fibers exhibit relatively high toughness (40–70 MJ m^{-3}) but suffer from significant creep deformation, leading to performance degradation under cyclic mechanical loading. Moreover, in the field of functional and intelligent fibers[2,5–7] for health monitoring/management, rehabilitation, and human-machine interaction applications, there is an urgent need to enhance the mechanical robustness or work capacity of emerging fiber-based electronic[8] and robotic devices[9,10] to meet practical textile requirements.

Natural spider silk stands out as an exemplary material system, uniquely combining high toughness (100–380 MJ m^{-3}) with exceptional strength (0.4–1.7 GPa), extensibility, and elastic recovery (up to 40% strain)[10,11]. These extraordinary mechanical properties enable spider silk to effectively capture prey and withstand mechanical impacts. Additionally, spider silk exhibits intelligent behaviors, such as reversible water absorption in response to environmental changes, and supercontraction, contracting up to 50% under high humidity or water exposure[12]. This property allows spider webs to restore their shape after deformation while maintaining tension for structural integrity. The major ampullate spider silk is mainly composed of proteins with molecular weights in the 250–400 kDa range, and its remarkable performance arises from its hierarchical protein structure, which includes microscale fibrillar structures, abundant spherical nanoclusters, and β-sheet nanocrystals with an orthorhombic lattice stabilized by intermolecular hydrogen bonds between amino and carbonyl groups[13–16] (Fig. 1a). The rigid β-sheet nanocrystals and aligned fibrils govern strength and stiffness, while the soft amorphous matrix contributes to ductility, entropic elasticity, and toughness. Furthermore, the abundance of polar amino acids enables moisture sensitivity, where hydrogen bonds between protein chains reversibly break and reform with humidity changes, driving supercontraction. To replicate the unique mechanical and intelligent behaviors of spider silk, tremendous efforts on synthetic artificial silk focus on mimicking the β-sheet nanocrystal function. Strategies include creating microphase-separated structures[17–23], and hybrid organic-inorganic composites of host-guest assembled networks[24,25], mineralized networks[25,26] or covalently crosslinked networks[27–29]. The heterogeneous structures of hard nanodomains embedded in a ductile matrix achieve high toughness alongside high strength. In addition, inducing orientation of multiscale oriented fibrous structures can further enhance mechanical performance[4,17,20,29–31]. Among artificial silk materials, hydrogel-based fibers have emerged as particularly promising due to their versatile functionalities, such as moisture sensitivity[18], environmental sensing[32,33], supercontraction[10,25], and artificial muscle actuation[9,22]. The highly tunable polymer networks and hygroscopic nature of those hydrogels closely resemble spider silk, making them ideal candidates for replicating its mechanical and intelligent behaviors. However, owing to the limited compatibility between hydrogel structure-function modulation and fiber spinning techniques[34], it remains a grand challenge to produce hydrogel fibers matching spider silk's properties, particularly ultrahigh toughness (hundreds of MJ m^{-3}) for impact resistance, textile-grade strength (hundreds of MPa), elastic recovery for durable mechanical loadings, and responsive supercontraction for smart actuation.

In this work, we present a strategy for engineering spider silk-like architectures and properties through controlled microphase separation and strain-programmed structural orientation in composite polymer hydrogel fibers. This scalable process is enabled by the conventional fiber manufacturing technique of wet-spinning combined with post- drawing (Fig. 1b). A uniform composite hydrogel dope composed of ultrahigh-molecular-weight (UHMW) sodium polyacrylate (PANa) and polyacrylamide (PAM) is extruded into a coagulating bath, where it undergoes antisolvent-induced phase separation to continuously produce nascent PANa-PAM fibers. UHMW PANa and UHMW PAM are commercially available, low-cost, and biocompatible polymers[35,36]. Their linear chain structures, devoid of complex side chains, feature carboxylic acid (PANa) and amide (PAM) groups. This structural composition enables the composite to form regular, compact hydrogen bonds, analogous to the β-sheet crystalline interactions in spider silk protein. The strong hydrogen bonding between carboxylic acid and amide groups induces microphase separation and generates hydrogen bond nanoclusters within the composite polymer network. This process can be precisely modulated by adjusting the hydrogel dope composition, pH, and antisolvent selection. Subsequent post-drawing under controlled strains introduces tensile stress along the fiber axis, promoting hydrogen bond reconstruction and enabling programmable multiscale structural alignment and crystallization. Conventional UHMWPE fibers suffer from low toughness and pronounced creep deformation owing to their lack of ductile, elastic components. In contrast, the bioinspired approach proposed in this work yields UHMW PANa-PAM composite hydrogel fibers that closely mimic the hierarchical architecture of natural spider silk, as illustrated in Fig. 1a,b, featuring aligned microfibrils, nanoscale hydrogen-bonded clusters, and crystallites with an orthorhombic unit cell similar to β-sheet crystallites in silk protein materials. Meanwhile, the process of biomimetic structure engineering aligning with fiber manufacturing enables scalable fabrication of tough yet strong microfibers ready for textile usage (Fig. 1c). This work establishes a pathway for creating spider silk-inspired fibers by wet-spinning UHMW composite polymers, achieving high performance and multifunctionality. Ashby diagrams comparing fracture strength versus modulus, fracture strain versus toughness, and damping capacity versus modulus across this work, reported fibrous materials, and natural spider silk can be found in Supplementary Fig. 1. Overall, optimized fibers exhibit comprehensive spider silk-like properties, including a toughness of 118.7 MJ m^{-3}, a fracture strength of 172.3 MPa, elastic recovery from 50% tensile strain, 96% damping capacity, 60% supercontraction, and moisture sensitivity, properties surpassing existing synthetic fibrous materials (Fig. 1d and Supplementary Table 1)[4,10,11,18,20,24,30,37,38].

Results

Controlled microphase separation in wet-spun composite polymer hydrogel fibers

Biomacromolecular phase separation within spiders produces β-sheet nanocrystals embedded in an amorphous matrix, which has greatly inspired transformative research on enhancing the mechanical properties of gel materials by transitioning from microstructural homogeneity to heterogeneity[39]. While significant efforts have been devoted to exploiting non-covalent interactions in polymer networks to induce microphase separation in gel materials, the regulation of such phase separation during a conventional wet-spinning process remains unexplored. Here, the hydrogel spinning dope was prepared by uniformly mixing UHMW PANa and PAM in deionized water. Under optimal conditions, these polymers are expected to form hydrogen bonds between the carboxylic acid groups of PANa and the amide groups of PAM, driving microphase separation within the resulting PANa-PAM composite network. In the traditional wet-spinning process, antisolvents are commonly used to induce polymer precipitation and produce nascent fibers. Apart from this effect, choosing antisolvents (poor solvents) is crucial for regulating the microphase separation of PANa-PAM composite hydrogel fibers. Upon injection into the coagulant bath, bidirectional diffusion occurs between water in the hydrogel dope and poor solvent from the bath, causing rapid accumulation of poor solvent within the composite networks. When the poor solvent concentration reaches a critical threshold, polymer aggregation is triggered, leading to rapid dehydration of the PANa-PAM hydrogel dope. This process significantly influences the hydrogen bonding interactions between PANa and PAM in the resulting fibers. Fig. 2a.i and Supplementary Movie 1 reveal that the formation of white polymer precipitates from the same PANa-PAM hydrogel dope (PAM/PANa

https://doi.org/10.1038/s41467-025-66537-7

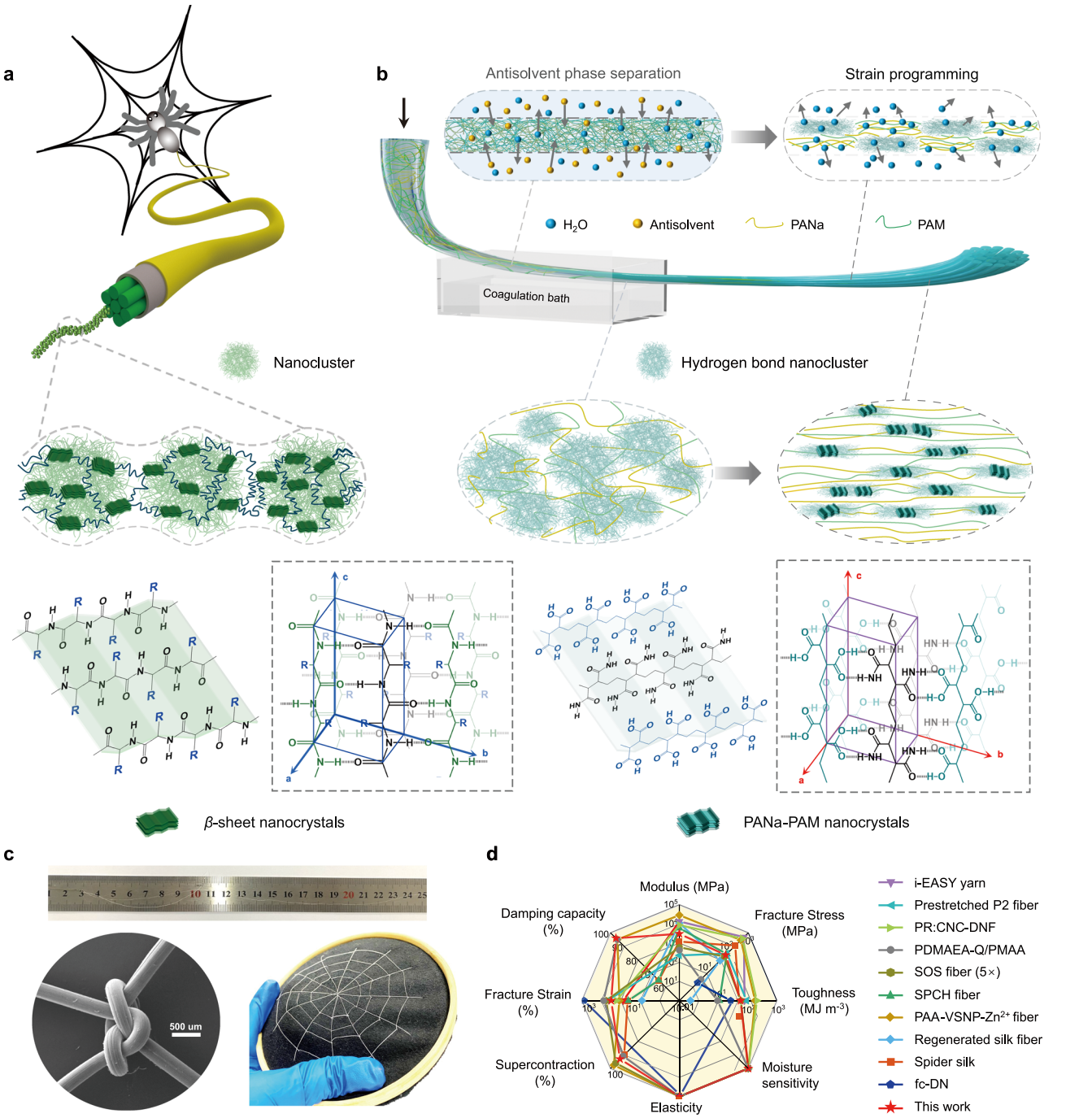

Fig. 1 | Bioinspired fabrication of PANa-PAM composite polymer hydrogel fibers with spider-silk like hierarchical architectures and properties. **a** Schematic illustration of the hierarchical structures of natural spider silk and (**b**) the bioinspired approach of wet-spinning combined with post-drawing that fabricate PANa-PAM hydrogel fibers via controlled microphase separation and strain programming. This process enables the fabrication of tough and strong fibers that exhibit a hierarchical structure resembling spider silk, including aligned microscale fibrils, hydrogen-bonded nanoclusters, and β-sheet-like crystallites analogous to those found in natural silk protein materials. **c** Scalable tough yet strong composite hydrogel fibers permitting complex knotting and direct sewing. **d** Properties comparison of our composite hydrogel fiber with spider silk[10,11] and reported biomimetic fibers including the i-EASY yarn[4], prestretched P2 fiber[10], PR:CNC-DNF fiber[18], PDMAEA-Q/PMAA fiber[20], SOS fiber (5×)[22], SPCH fiber[24], PAA-VSNP-Zn^{2+} fiber[30], regenerated silk fiber[37], and fc-DN[38].

mass ratio = 1/2, pH 4.1) occurs more rapidly and distinctly in antisolvents with higher polarity (methanol > ethanol > isopropyl alcohol). The mechanical properties of PANa-PAM fibers were measured at a relative humidity (RH) of 65% and a strain rate of 2 throughout unless stated otherwise. Notably, the resulting PANa-PAM fibers exhibit progressively enhanced strength and modulus without significantly compromising extensibility. As the antisolvent is varied from isopropyl alcohol (IPA) to ethanol (EtOH) and to methanol (MeOH), the elastic modulus increases significantly from 81.7 MPa to 155.0 MPa and to 252.9 MPa, respectively (Fig. 2a.ii). Notably, using a methanol/water mixed antisolvent (optimal mass ratio of 7:3) further enhanced the mechanical properties of PANa-PAM hydrogel fibers. As water content increases from 10 wt% to 20 wt% and 30 wt%, fiber strength and modulus continuously increase, achieving an elastic modulus of 455.6 MPa, fracture strength of 17.5 MPa, and fracture strain of 290.5% with the methanol/water mixture (7:3 mass ratio) (Supplementary

https://doi.org/10.1038/s41467-025-66537-7

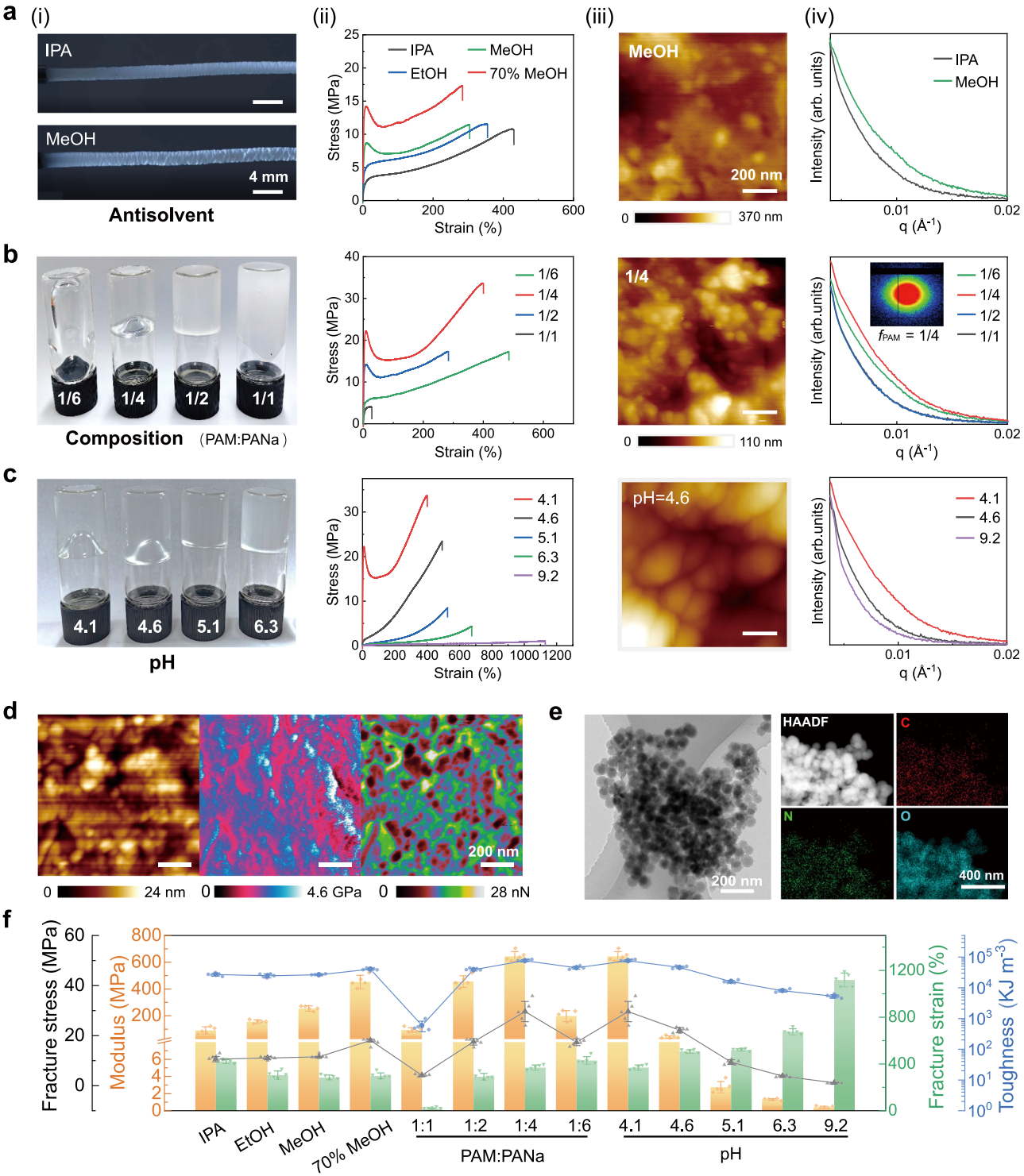

Fig. 2 | Antisolvent-induce phase separation for controlled microphase separation in wet-spun nascent PANa-PAM hydrogel fibers. a The effect of antisolvent on fiber structure and properties. (i) Optical microscope images showing composite hydrogel filamentation in IPA and EtOH. (ii) Stress-strain curves of PANa-PAM fibers (f_{PAM} = 1/2, pH 4.1) precipitated from different antisolvents. (iii) An AFM image for the PANa-PAM fiber processed from MeOH. (iv) 1D SAXS profiles of PANa-PAM fibers precipitated from IPA and MeOH. **b** The effect of polymer composition on fiber structure and properties. (i) Photos of PANa-PAM hydrogel dopes (pH = 4.1) with different f_{PAM} and (ii) stress-strain curves of the resulting fibers. (iii) An AFM image of the PANa-PAM fiber with f_{PAM} = 1/4. (iv) 1D SAXS profiles of PANa-PAM fibers with different f_{PAM}. **c** The effect of hydrogel dope pH on fiber structure and properties. (i) Photos of PANa-PAM hydrogel dopes (f_{PAM} = 1/4) at different pH and (ii) stress-strain curves of the resulting fibers. (iii) An AFM image of the PANa-PAM fiber processed from hydrogel dope of pH 4.6. (iv) 1D SAXS profiles of PANa-PAM fibers processed from hydrogel dopes of different pH. **d** PeakForce quantitative nanomechanical AFM analysis for the PANa-PAM fiber with an optimized microphase separation structure in terms of nanoscale morphology, modulus, and adhesion force. **e** TEM image, HAADF image and elemental maps of the optimized PANa-PAM fiber. **f** Mechanical properties tunability of PANa-PAM fibers based on controlled microphase separation. The dots of different colors represent the measured data points. Data are presented as mean ± standard deviation from n = 5 independent samples.

Fig. 2). This effect might be attributed to the fact that hydrogels in a mixture of poor/good solvent usually achieve the optimal microphase separation structure for mechanical reinforcement[40]. Atomic force microscope (AFM) imaging reveals microphase-separated nanostructures in methanol-derived PANa-PAM hydrogel fibers, featuring hydrogen-bonded polymer-rich nanoclusters with sizes within 100 nm (Fig. 2a.iii and Supplementary Fig. 3). These nanoclusters are absent in fibers precipitated with EtOH or IPA. Small-angle X-Ray scattering (SAXS) analysis confirms the structural heterogeneity through distinct polymer-rich nanoclusters surrounded by polymer sparse regions, with methanol-processed fibers showing significantly stronger scattering intensity (Fig. 2a.iv and Supplementary Fig. 4). Additionally, scanning electron microscope (SEM) imaging was employed to characterize the macroscopic and microscale morphologies of the fibers. The hydrogel fiber surfaces become progressively smoother as the antisolvent polarity increases from isopropanol to ethanol to methanol, respectively. Fibers containing polymer-rich nanoclusters fabricated using the methanol/water mixture (7:3) show the ultimate microscale smoothness without macroscopic wrinkles (Supplementary Fig. 5). This reduction in surface roughness and microstructural defects likely contributes to the observed mechanical enhancement.

To further optimize the microphase structures arising from hydrogen bonds between PAM and PANa, we investigated PANa-PAM hydrogel fibers with varying polymer compositions. By maintaining a constant PANa concentration (0.073 g ml^{-1}, pH 4.1), we prepared composite hydrogel dopes with different PAM/PANa mass ratios (f_{PAM}). As f_{PAM} increases, the hydrogel dopes transition from transparent to translucent and finally to opaque (Fig. 2b.i), demonstrating significant microphase separation driven by enhanced hydrogen bonding between PAM and PANa (Supplementary Fig. 6 and Supplementary Movie 2). All hydrogel dopes exhibit viscoelastic behavior with shear-thinning properties. The apparent viscosity initially increases as f_{PAM} rises from 1/6 to 1/2 but decreases upon further increase to 1 (Supplementary Fig. 7). Strain-dependent oscillatory rheology measurements reveal the highest storage modulus (G′ = 365 Pa) in the linear viscoelastic region for the composite hydrogel dope at f_{PAM} = 1/2, and the gradual decrease in gel-to-sol crossover points with increasing f_{PAM} may result from enhanced strain sensitivity due to stronger hydrogen bonding interactions within the gel networks (Supplementary Fig. 8). Fourier-transform infrared spectroscopy (FT-IR) analysis (Supplementary Fig. 9) reveals enhanced hydrogen bonding interactions in the composite polymer network. The absorption band at 1630 cm^{-1} corresponds to C=O stretching, while the peak at 1401 cm^{-1} arises from COO^- stretching in PANa. With the incorporation of PAM, distinct NH_2 stretching vibrations emerge at 3235 cm^{-1} and 3417 cm^{-1}. Additionally, the appearance of two bands at 3547 cm^{-1} and 3475 cm^{-1} suggests the formation of extensive intramolecular and intermolecular hydrogen bonds. Temperature-dependent FT-IR reveals the gradual dissociation of hydrogen bonds associated with carboxylic acid groups and amide groups within PANa-PAM fibers during heating (Supplementary Fig. 10). Mechanical measurements reveal that PANa-PAM fibers exhibit significantly enhanced strength and modulus with minimal loss of extensibility as f_{PAM} increases from 1/6 to 1/4. However, further increasing f_{PAM} leads to a decline in mechanical performance. At f_{PAM} = 1, the fibers become brittle, showing the lowest strength, modulus, and extensibility (Fig. 2b.ii). AFM imaging reveals distinct microphase separation, with abundant spherical nanoclusters (50–100 nm) at f_{PAM} = 1/4 (Fig. 2b.iii). As f_{PAM} further increases, these nanoclusters tend to grow in size and adopt irregular morphologies (Supplementary Fig. 11). SAXS analysis confirms the strongest scattering intensity in PANa-PAM fibers at f_{PAM} = 1/4 (Fig. 2b.iv and Supplementary Fig. 12), indicating the optimal microphase-separated structure with dense, well-defined nanoclusters that significantly enhance fiber toughness and strength. Additionally, the ellipsoidal SAXS pattern (inset, Fig. 2b.iv) indicates an axial orientation of polymers along the fiber axis, resulting from the extrusion and shear forces experienced during the spinning process (Supplementary Fig. 13). The translucent/opaque hydrogel dopes at f_{PAM} = 1/2 and 1 produce PANa-PAM fibers with large and irregular polymer aggregates, which tend to embrittle the composite networks. SEM observations for the fibers with varying polymer compositions support this result. The composite fibers with high contents of PAM (f_{PAM} = 1/2 and 1) exhibit nonuniform, rough surface microstructures (Supplementary Fig. 14), which likely cause stress concentration during fiber stretching at low strains.

The hydrogen bonds in PANa-PAM hydrogel fibers can be well controlled by modulating the protonation state of carboxylate groups in PANa. At pH 4.1, the globule chain conformation of PANa and the protonated carboxylate groups facilitate the formation of hydrogen bond nanoclusters. AFM images for the pH 4.1 fiber in Supplementary Fig. 15 show the optimized microphase separation structure at different magnifications. However, even a slight increase in pH significantly weakens microphase separation. For composite hydrogel dopes (f_{PAM} = 1/4), the viscosity and storage modulus exhibit a continuous increase as pH rises from 4.1 to 9.2 (Fig. 2c.i and Supplementary Figs. 16 and 17) attributed to the globule-to-coil conformational transition of PANa chains, consistent with earlier findings[32]. Notably, when pH increases marginally from 4.1 to 4.6, the stress-strain curves undergo a dramatic change, with the elastic modulus dropping sharply from 643.8 to 39.4 MPa. Across the pH range of 4.1 to 9.2, PANa-PAM fibers exhibit progressively reduced strength and modulus but enhanced extensibility (Fig. 2c.ii). AFM imaging reveals corresponding nanostructural changes: as pH increases, the heterogeneity of the composite network progressively decreases. Concurrently, the size of the microphase-separation nanoclusters increases, while their number significantly decreases (Fig. 2c.iii and Supplementary Fig. 18). At pH 9.2, the fiber exhibits a homogeneous nanostructure devoid of aggregated nanoclusters. These observations align with SAXS analysis, which shows a decrease in scattering intensity as pH increases (Fig. 2c.iv and Supplementary Fig. 19). The SAXS 1D curve fitting results for the fiber at pH = 4.1 show $q^{-3.95}$ scaling, indicating the presence of molecular chain scattering originating from hydrogen bond nanoclusters with well-defined interfaces[20] (See more details in Supplementary Fig. 20). Quantitative nanomechanical AFM imaging was applied to reveal the modulus contrast between polymer-rich nanoclusters stabilized by dense hydrogen bonding and polymer-sparse regions lacking strong interactions. As shown in Fig. 2d, the nanoclusters observed in the topography image correspond to the high-brightness regions in the modulus map, with values ranging from 2.1 to 4.5 GPa. In contrast, the surrounding regions exhibit a lower modulus of 0.7 to 2.1 GPa. In the adhesion map, the nanoclusters well align with areas of reduced adhesion force, indicating that these clusters possess enhanced stiffness and smoother surfaces. Quantitative nanomechanical AFM imaging for fibers with different microphase separation structures shown in Supplementary Fig. 21 reveals consistent results. Transmission electron microscopy (TEM) imaging reveals nanoclusters with well-defined spherical morphologies, whose distribution characteristics closely match those observed in the AFM images (Fig. 2e). High-angle annular dark field (HAADF) image demonstrates a densely packed arrangement of clusters, exhibiting structural similarities to silk protein assemblies. Elemental mapping confirms a uniform distribution of C, N, and O, originating from the intermolecular hydrogen bonding between PANa and PAM.

Taken in sum, the microphase separation governed by hydrogen bond nanoclusters in wet-spun PANa-PAM composite polymer hydrogel fibers can be effectively modulated by adjusting the antisolvent, polymer composition, and hydrogel dope pH (Fig. 2f and Supplementary Table 2). Under optimized conditions (f_{PAM} = 1/4, pH = 4.1, and precipitation in a methanol/water mixture with a 7:3 mass ratio), the resulting PANa-PAM fibers exhibit exceptional stiffness and

https://doi.org/10.1038/s41467-025-66537-7

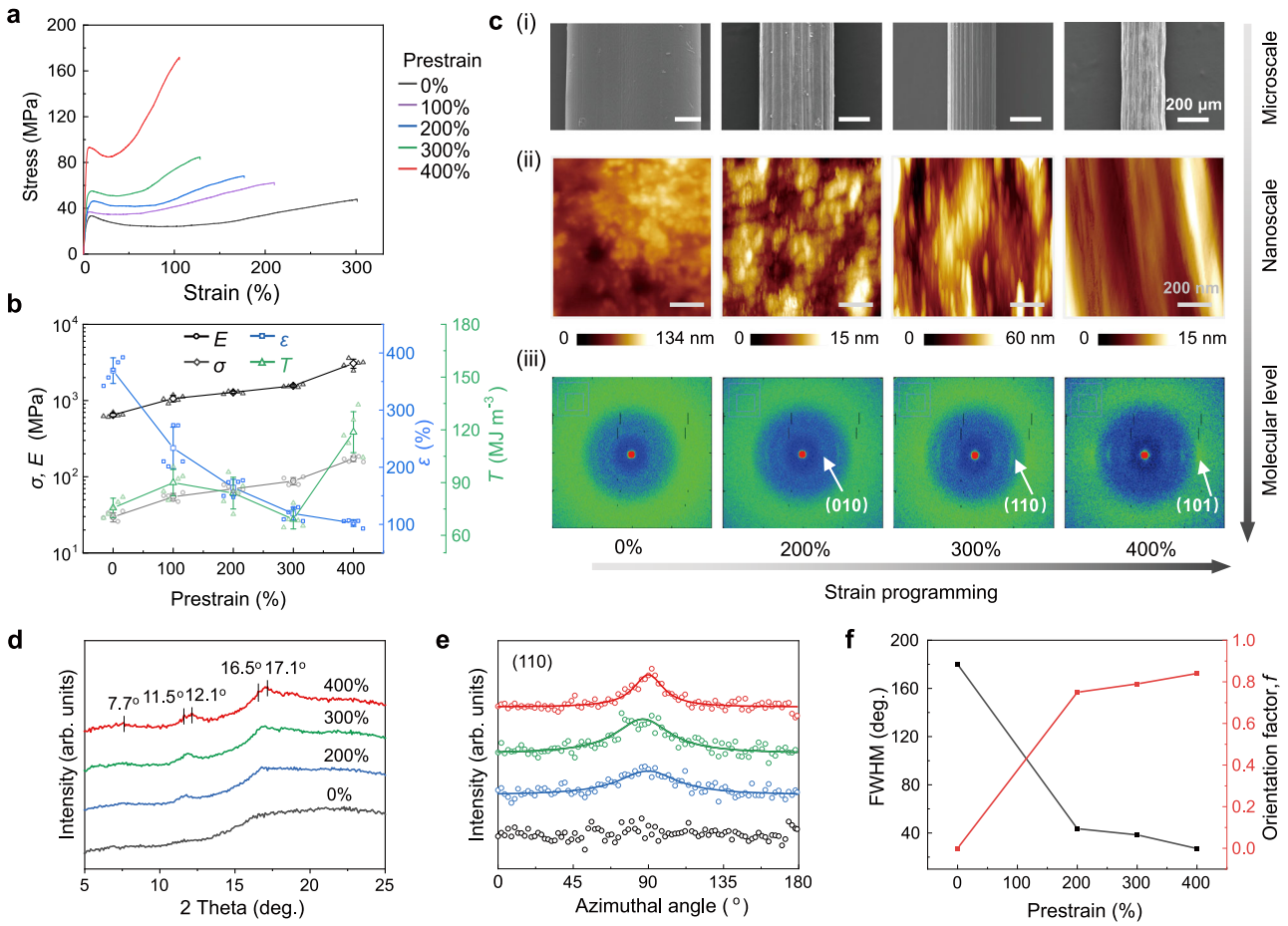

Fig. 3 | Post-drawing enabled strain programming for uniaxial orientation and controlled crystallization in PANa-PAM hydrogel fibers. a Stress–strain curves, (**b**) mechanical properties and (**c**) multiscale structures of prestrained PANa-PAM fibers. Fracture stress, fracture strain, elastic modulus, and toughness are respectively represented by σ, ε, E, and T. All data were tested for five times, and the error bars are presented as mean ± standard. (i) SEM images, (ii) AFM images and (iii) 2D WAXS patterns of prestrained PANa-PAM fibers. **d** 1D WAXS profiles perpendicular to the fiber axis of prestrained PANa-PAM fibers. **e** Azimuthally dependent scattering spectra at $2\theta = 12.1°$ and (**f**) full width at half maximum (FWHM) of azimuthal peaks and orientation factor calculation at different prestrains.

toughness, achieving a fracture stress of 29.6 MPa, an elastic modulus of 643.8 MPa, a fracture strain of 369.4%, and a toughness of 75.6 MJ m^{-3}. Notably, pH adjustment enables wide control over structural heterogeneity of the composite polymer network, allowing for a broad spectrum of mechanical properties. For instance, soft and highly stretchable PANa-PAM fibers prepared at pH 9.2 display an elastic modulus of 0.39 MPa and an extraordinary fracture strain of 1120.2%.

Post-drawing for strain programming in microphase-separated hydrogel fibers

After extrusion from the spinneret, the spider silk fibers are mechanically post-drawn by the spider's legs, significantly enhancing their axial molecular alignment. This ordered, hierarchical microstructure is a hallmark of high-performance natural uniaxial materials[41,42]. In both biological and synthetic spinning processes, inducing such uniaxial alignment is critical for producing fibers with high strength and stiffness. The PANa-PAM hydrogel fibers with an optimized microphase-separated structure underwent strain programming via post-drawing to introduce varying degrees of molecular orientation and crystallization. During this process, the PANa-PAM fiber was prestretched at 100% to 400% strain in a 75% RH environment to align the polymer chains, followed by stabilization at 65% RH for ≈6 h to fix the aligned structure. Tensile stress-strain curve of the fiber at 75% RH is shown in Supplementary Fig. 22. As shown in Fig. 3a, increasing the prestrain leads to progressively higher strength and stiffness but reduced stretchability. The 400% prestrained PANa-PAM (PANa-PAM-400%) fiber achieves a fracture stress of 172.3 MPa, an elastic modulus of 3.05 GPa, and a maximum toughness of 118.7 MJ m^{-3} (Fig. 3b and Supplementary Table 3). These mechanical properties are comparable to those of spider silk, and remain highly stable over a 28-day measurement period (Supplementary Fig. 23). Meter-scale PANa-PAM-400% fibers were successfully fabricated, and demonstrated excellent knotability in various configurations (Supplementary Fig. 24).

We systematically investigated the multiscale structural changes in the strain-programmed composite polymer fibers. Under polarized light, the fibers exhibit pronounced birefringence, with interference colors shifting from yellow to purple as prestrain increases, reflecting enhanced polymer alignment (Supplementary Fig. 25)[43]. SEM imaging shows a progressive reduction in fiber width, from an original 820 μm to ≈450, 310, and 270 μm at 200%, 300%, and 400% prestrain, respectively (Fig. 3c.i). Simultaneously, the initially smooth surface develops uniaxially oriented textures, forming densely aligned microfibrillar structures as polymer chains reorganize into bundled microfibers at higher prestrains. The nanostructural evolution induced by increasing prestrain was systematically characterized using AFM (Fig. 3c.ii and Supplementary Fig. 26). In contrast to the original PANa-PAM fiber featuring randomly distributed nanoclusters, the PANa-

PAM-200% fiber exhibits significantly enlarged nanoclusters, suggesting a reconstruction of hydrogen-bonded networks under stressed, high-humidity conditions, and the phase contrast between nanocluster-rich and amorphous regions was decreased. The PANa-PAM-300% fiber demonstrates highly elongated nanoclusters aligned along the fiber axis, clearly evidencing both microphase separation and structural alignment. Notably, nanoclusters become virtually indistinguishable in the PANa-PAM-400% fiber, likely due to extreme alignment and densification of polymer chains. Complementary 2D SAXS patterns show progressively intensified diffraction perpendicular to the fiber axis with increasing prestrain (Supplementary Fig. 27), further corroborating nanoscale structural alignment. The wide-angle X-ray scattering (WAXS) measurements offer further evidence of molecular-scale reorganization (Fig. 3c.iii and d). The as-prepared PANa-PAM fiber shows only weak diffraction peaks, suggesting a low degree of crystallinity in the absence of post-drawing treatment. As the prestrain increases from 200% to 400%, the diffraction peaks become more intense. The asymmetric peak shapes indicate the presence of overlapping reflections. Specifically, the WAXS profile of the PAA-PAM fiber under 400% prestrain displays diffraction peaks at $2\theta = 7.7°$, 11.5°, 12.1°, 16.5°, and 17.1°. Among these, the peaks at 11.5° and 16.5° are assigned to the (110) and (101) reflections, respectively, of polyacrylic acid (PAA) crystals with an orthorhombic unit cell, consistent with previous reports[44,45] and also observed in the pure PANa fiber (Supplementary Fig. 28). The remaining peaks at $2\theta = 7.7°$, 12.1°, and 17.1° are attributed to the (010), (110), and (101) reflections, respectively, of a PAA-PAM co-crystal structure. These reflections correspond to an orthorhombic unit cell with slightly different parameters than those of pure PAA crystals (Supplementary Table 4). Quantitative analysis of the azimuthal intensity distribution for the (110) reflection yields the crystallite orientation parameters (Fig. 3e, f). The orientation factor (f) evolves from near-isotropic ($f \approx 0$) in the unstretched state to highly aligned ($f = 0.84$) at 400% prestrain. Post-drawing for strain programming under stressed, high-humidity conditions induces pronounced alignment and oriented crystallization of the composite polymer chains, which in turn guides the formation of highly oriented nanoclusters and microfibrils along the fiber axis while simultaneously enhancing composite polymer crystallization within the nanoclusters. The resulting PANa-PAM-400% fiber integrates aligned microscale fibrils composed of orientated polymer chains, rigid hydrogen-bonded nanoclusters surrounded by softer polymer-sparse domains, and composite polymer crystallinity analogous to β-sheet crystals in silk protein. This sophisticated hierarchical architecture enables the fiber to closely replicate both the structural complexity and mechanical characteristics of natural spider silk.

Spider silk-like attributes of composite polymer hydrogel fibers

With high structural similarity to spider silk, the PANa-PAM-400% fibers not only replicate the exceptional toughness and strength of spider silk but also possibly acquire a range of advanced functionalities, including shock resistance, moisture sensitivity, elastic recovery, energy absorption, and supercontraction. We systematically evaluated these spider silk-like behaviors in PANa-PAM-400% fibers. Dragline silk serves as a lifeline for spiders, enabling critical functions including body weight support, locomotion, controlled descent from heights, and prey capture, all of which demand high strength and stiffness under both static and dynamic loading conditions (Fig. 4a, left). The PANa-PAM-400% fibers demonstrate high load-bearing capacity, with a single 9.2 mg fiber (cross-sectional area of ≈0.5 mm^2) supporting a 1 kg static load, approximately 110,000 times its own weight (Fig. 4a, right), surpassing most reported biomimetic fibers[20,33,43,46,47]. Progressive increases in stretching rate from 10 to 160 mm/min result in corresponding enhancements of elastic modulus from 1.98 to 4.32 GPa and yield stress from 63.5 to 152.9 MPa (Fig. 4b, c). Consequently, these fibers exhibit enhanced deformation resistance and higher load-bearing capacity at elevated strain rates, making them particularly suitable for protective applications under dynamic mechanical conditions. Natural spider silk exhibits significant moisture sensitivity due to its high content of hygroscopic amino acids. Similarly, the PANa-PAM-400% fiber containing amide and carboxylate groups demonstrates comparable hygroscopic properties. Under identical environmental conditions, the PANa-PAM-400% fiber shows higher water content than spider silk, reaching ≈23 wt% at 65% RH, approximately twice that of natural spider silk (Fig. 4d)[48]. As relative humidity decreases, the fiber exhibits increased stiffness and strength but reduced extensibility (Supplementary Fig. 29a, b). At 55% RH, the fracture strength and modulus of the fiber with ≈13 wt% water content reach 231.2 MPa and 3.91 GPa, respectively, while the fracture strain remains relatively high at 77.6%. The J-shaped stress-strain curve observed at 85% RH suggests that hydrogen bond clusters persist as robust crosslinks within the composite network, enabling effective strain stiffening under high tensile deformation (Supplementary Fig. 29c). The damping properties of spider silk enable effective shock absorption during high-velocity prey capture, preventing prey rebound through efficient energy dissipation. Our cyclic loading tests reveal high energy dissipation performance of the biomimetic fiber (Fig. 4e), with the damping capacity stably maintaining at ≈96% across 20–100% strain, and the dissipated energy at 100% strain reaches 116.4 MJ m^{-3} (Fig. 4f). Progressive loading tests demonstrate consistent enhancement of energy absorption, where stepwise 20% strain increments from 20% to 100% strain yield steadily increasing energy dissipation (Supplementary Fig. 30). The spider silk is damping yet elastic, enabling restoration of both shape and mechanical properties following energy absorption. The PANa-PAM-400% fiber exhibits substantial residual strain exceeding 40% and strength degradation following initial loading to 50% strain, accompanied by a significant reduction in energy dissipation capacity (Fig. 4g). However, moisture treatment followed by stabilization at 65% RH facilitates structural reorganization, resulting in full recovery of both mechanical properties and damping performance. Notably, under elevated humidity conditions (85% RH), the fiber demonstrates exceptional elastic recovery and maintains consistent mechanical stability throughout repeated 100% strain loading cycles (Supplementary Fig. 31). Figure 4h demonstrates that a single PANa-PAM-400% fiber hanging a load 50,000 times its own mass effectively absorbs impact energy from free-falling weights at varying heights. The fiber rapidly dissipates vibrational energy, bringing the oscillating mass to complete rest within seconds. With a 96% damping capacity coupled with elastic recovery from 50% tensile strain, surpassing the performance of spider silk (damping capacity of 50–70%)[48,49] as well as most other natural and synthetic materials[25], the PANa-PAM-400% fiber represents the state-of-the-art in high-performance damping materials for energy absorption applications.

The supercontraction of spider silk under high humidity or water exposure primarily results from the disruption of intermolecular hydrogen bonds, which leads to molecular chain disorientation and subsequent recoiling[50]. Inspired by this mechanism, we expected that strain-programmed PANa-PAM fibers with rich hydrogen bonds and aligned polymer chains should exhibit similar supercontraction behavior through the breakdown of their hydrogen-bonded composite network. To test this, we applied thermal (100 °C) and moisture (85% RH) stimuli to induce supercontraction in PANa-PAM fibers with varying degrees of structural alignment (Fig. 5a). The actuation strain increases with the prestrain level, attributed to the greater contraction distance of more aligned PANa chains. Thermal stimulation produces higher actuation strains than moisture for the same fiber, with the PANa-PAM-400% fiber reaching 57% at 100 °C. As shown in Fig. 5b, thermal actuation stress increases from 0.4 to 2.4 MPa as prestrain

https://doi.org/10.1038/s41467-025-66537-7

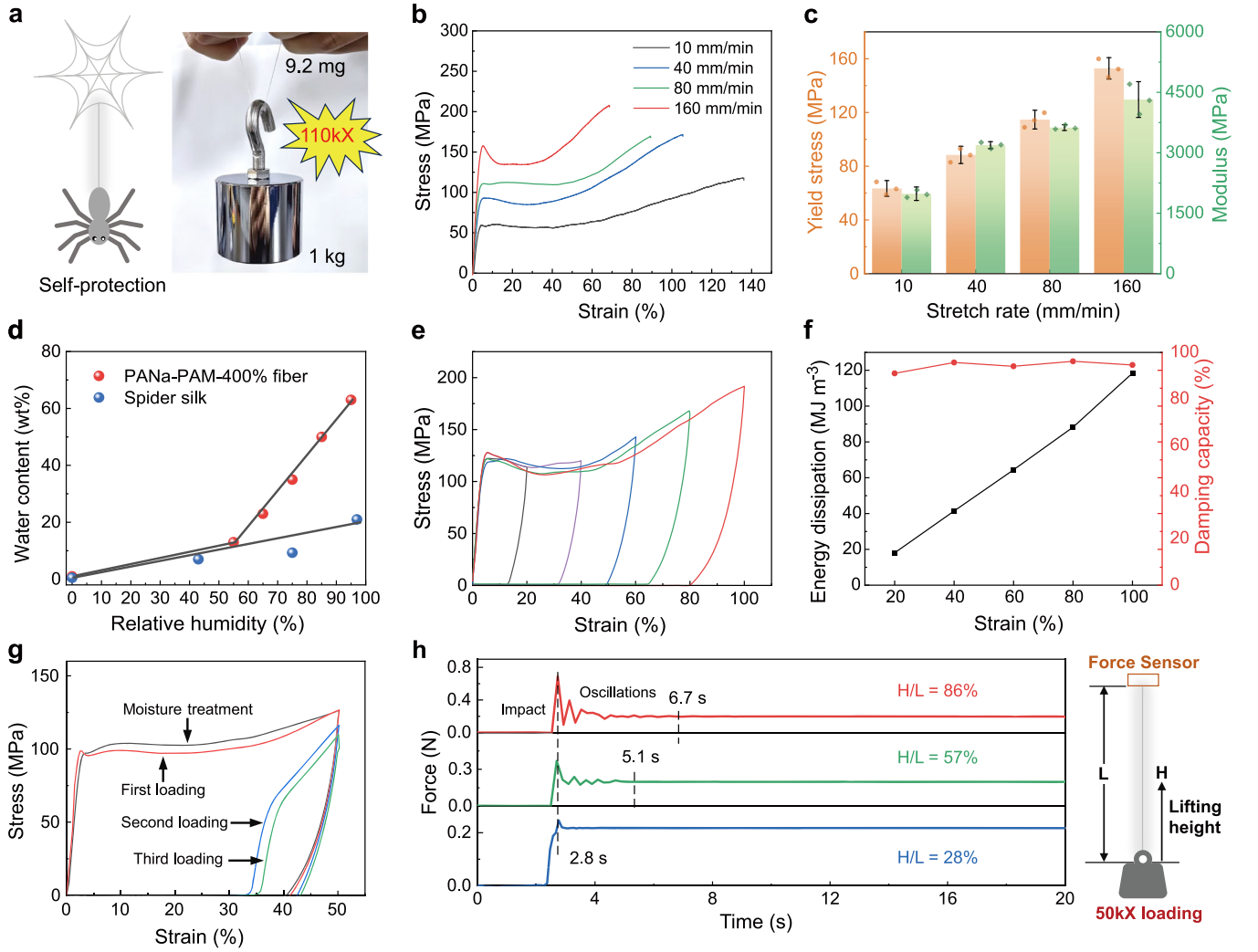

Fig. 4 | Spider silk-like loading bearing, moisture sensitivity, damping-yet-elastic properties of PANa-PAM-400% fibers. a Schematic illustration of spider silk hanging its body for self-protection and a photo of the biomimetic fiber hanging a static load of 1 kg (right). **b** Stretching rate-dependent stress-strain curves and (**c**) yield stress and elastic modulus of the biomimetic fiber. The dots of different colors represent the measured data points of three. Error bars are presented as mean ± standard deviation from $n = 3$ independent samples. **d** The effect of relative humidity on water retention capability of spider silk[48] and the biomimetic fiber. **e** Cyclic stress-strain curves of the biomimetic fiber within 20–100% strain. **f** The dissipated energy and damping capacity within 20–100% strain. **g** The cyclic stress-strain curves with and without moisture treatment. **h** Time-dependent impact force oscillations of a free-falling object from different heights damped by the biomimetic fiber.

rises from 100% to 400%. Higher prestrains also accelerate actuation, with stress peaking within ≈3 s. Temperature-dependent studies revealed that supercontraction in the PANa-PAM-400% fiber was not triggered at 40 °C. However, increasing the temperature from 60 to 120 °C enhances actuation strain from 3% to 60%, while the actuation stress at 120 °C reaches 3.2 MPa (Supplementary Fig. 32). To further enhance the actuation performance, we applied a secondary prestrain (100%) to the PANa-PAM-400% fiber, yielding the PANa-PAM-400%×2 fiber. This modification improves thermal sensitivity and actuation strain, with the actuation strain reaching 18% at 40 °C and 69% at 120 °C (Fig. 5c). More strikingly, the actuation stress of PANa-PAM-400%×2 increases by over an order of magnitude compared to PANa-PAM-400% at the same temperature, reaching 42 MPa at 120 °C versus 3.2 MPa for the untreated fiber (Fig. 5d). This suggests substantially greater stress storage in the highly stretched and aligned polymer chains after secondary prestretching. We assessed the work capacity of the prestrained fibers by performing weight-lifting tests at 120 °C. As expected, both actuation stroke and work capacity of the fibers increases with prestrain (Fig. 5e). The PANa-PAM-400%×2 fiber rapidly contracts under a load >1000 times its own mass (Fig. 5f and Supplementary Movie 3), achieving ≈54% actuation stroke and a work capacity of 516 J kg^{-1}, far surpassing biological muscle (39 J kg^{-1})[51]. Additionally, the thermal supercontraction can promote the mechanical properties recovery of the tough and strong PANa-PAM-400% fibers. After energy dissipation at 50% tensile deformation, ≈45% residual strain is fully recovered via heating (120 °C)-induced supercontraction followed by stabilization at 65% RH. The fiber maintains consistent mechanical performance over ten energy absorption cycles (Fig. 5g). Supplementary Movie 4 demonstrates that the PANa-PAM-400% fiber after large deformation recovered by thermal supercontraction can still stably bear a 1 kg load. These findings highlight the high reversibility of hydrogen bond reorganization that drives repeatable supercontraction in our biomimetic composite polymer hydrogel system (Fig. 5h).

Discussion

In summary, we report PANa-PAM composite polymer hydrogel fibers with spider silk-like architectures and properties, fabricated via

https://doi.org/10.1038/s41467-025-66537-7

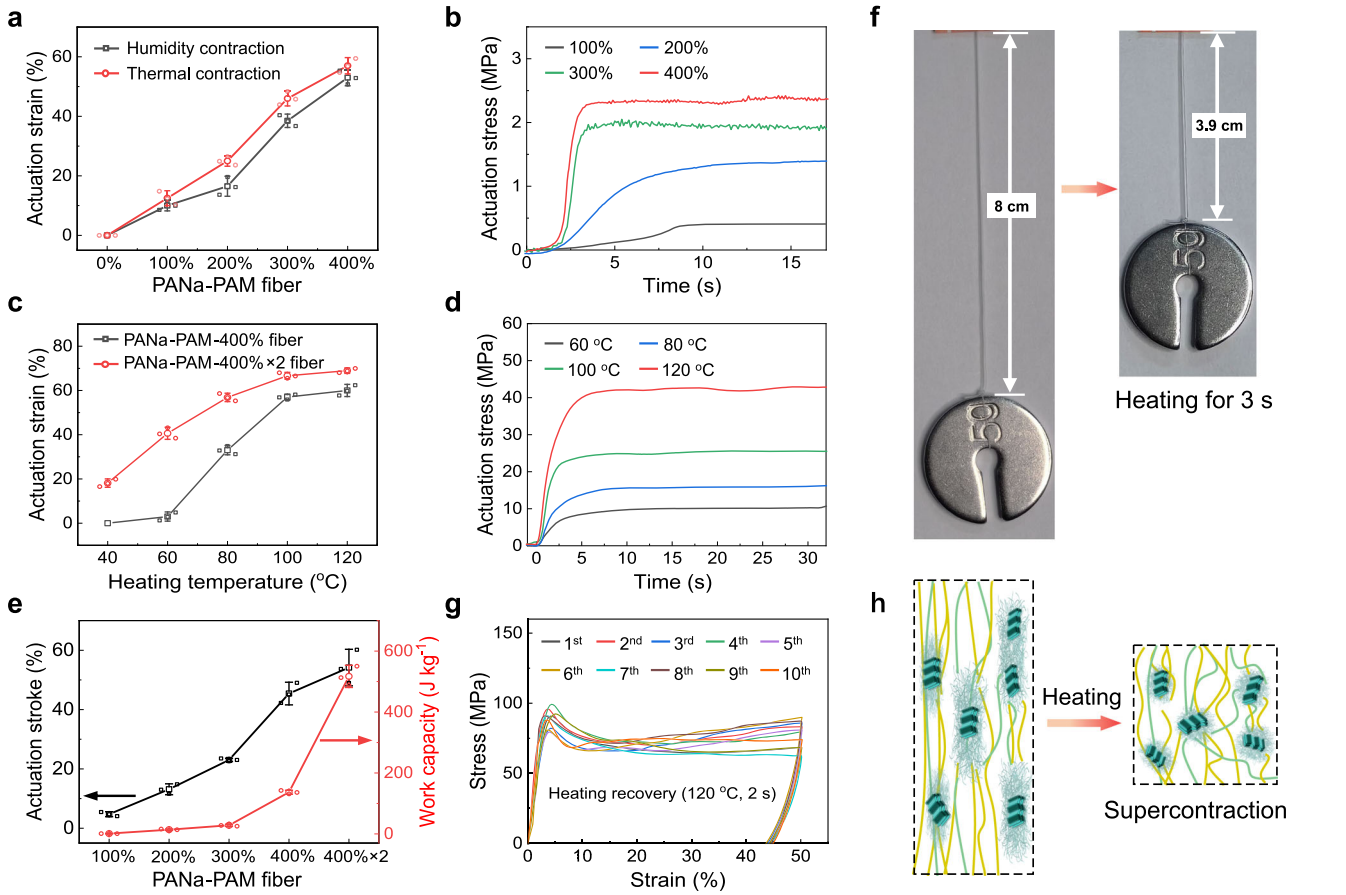

Fig. 5 | The supercontraction performance of prestrained PANa-PAM hydrogel fibers. a Actuation strain of PANa-PAM hydrogel fibers processed with different prestrains induced by moisture (85% RH) or thermal supercontraction (100 °C). **b** Actuation stress of prestrained PANa-PAM fibers induced by heating at 100 °C. **c** Actuation strain of the PANa-PAM-400% fiber and PANa-PAM-400%×2 fiber as a function of heating temperature. **d** Actuation stress of the PANa-PAM-400%×2 fiber at different heating temperatures. **e** Actuation stroke and work capacity of prestained PANa-PAM fibers. **f** Photos showing the thermal supercontraction (120 °C) of PANa-PAM-400%×2 fiber lifting a 5 g load. **g** Cyclic stress-strain curves of the PANa-PAM-400% fiber with thermal treatment. **h** Schematic illustration of the structural changes of the strained PANa-PAM fiber for supercontraction. All data in (**a**, **c**, **e**) were tested for three times and the error bars are presented as mean ± standard.

conventional wet-spinning. The composite polymers of UHMW PANa and PAM are selected, as the hydrogen bonds between the carboxylic acid and the amide group drive polymer microphase separation at suitable conditions. The antisolvent-induced phase separation process determined by the hydrogel dope composition, pH, and antisolvent selection controls the microphase separation, modulating hydrogen-bonded PANa-PAM nanoclusters within the composite polymer network, while the post-drawing under a high-humidity condition enables strain programming to engineer uniaxial structural alignment and composite polymer crystallization. The optimized PANa-PAM-400% fiber integrates aligned microscale fibrils composed of oriented polymer chains, nanoclusters of PANa-PAM polymer-dense domains surrounded by polymer-sparse regions, and β-sheet-like composite polymer crystallization, well mimicking the hierarchical architecture of spider silk. Consequently, it achieves comprehensive spider silk-like properties and functionalities unmatched by existing synthetic fibers, including a toughness of 118.7 MJ m^{-3}, a fracture strength of 172.3 MPa suitable for textile usage, 50% elastic strain, 96% damping capacity, thermal/moisture supercontraction with over 60% actuation strain, and moisture sensitive mechanical properties. These findings provide a bioinspired, fiber manufacturing-compatible strategy to tailor biomimetic multiscale structures in composite polymer hydrogels, advancing high-performance and functional fibers for smart wearable technologies.

Methods

Materials

Sodium polyacrylate (PANa, $M_w \approx 3 \times 10^7$ Da), polyacrylamide (PAM, $M_w \approx 1.2 \times 10^7$ Da), methyl alcohol (MeOH), ethanol (EtOH), and isopropanol (IPA) were purchased from Sinopharm Chemical Reagent Co. Ltd. Concentrated hydrochloric acid (HCl) was purchased from Shanghai Lingfeng Chemical Reagent Co., Ltd. Deionized water was used in all experiments.

Preparation of hydrogel spinning dopes

The PANa powder was dissolved in 20 mL of 0.5 M HCl under magnetic stirring at 70 °C for 5 min until complete polymer swelling was achieved, yielding PANa gels with a fixed concentration of 0.073 g ml^{-1}. HCl was used to adjust the protonation state of carboxyl groups ($-COO^-$) in PANa. Subsequently, varying ratios of PAM powder were gradually added to the swollen matrix under continuous mechanical agitation at 65 °C for 6 h, forming a uniform hydrogel. Finally, the hydrogel spinning dope was obtained by high-speed centrifugation to remove entrapped air bubbles.

Preparation of PANa-PAM fibers with controlled microphase separation

The PANa-PAM hydrogel spinning dope was extruded through an 18 G needle (outer diameter: 3 mm) into a coagulation bath at a constant

injection rate of 0.15 mL min^{-1}. The fibers were collected tension-free using a synchronized-speed collector and equilibrated under ambient humidity (65% RH) for 8 h to achieve moisture equilibrium, yielding the final PANa-PAM fibers. To study the influence of antisolvent on fiber structure and properties, hydrogel dopes (f_{PAM} = 1/2, pH 4.1) were spun and precipitated in MeOH, EtOH, IPA, and MeOH/water mixed solutions. To examine the effect of polymer composition, hydrogel spinning dopes (pH 4.1) with f_{PAM} ranging from 1/6 to 1 were spun and precipitated in a methanol/water mixture (mass ratio 7:3). To assess the impact of pH, hydrogel dopes (PAM/PANa mass ratio = 1/4) with pH values from 4.1 to 9.2 were spun and precipitated in the same methanol/water mixture (7:3).

Strain programming in PANa-PAM fibers

The PANa-PAM fibers (f_{PAM} = 1/4, pH 4.1), precipitated from the MeOH/water (7:3) coagulation bath, were retrieved and subjected to prestretching at a constant rate (20 mm min^{-1}) with incremental strains ranging from 100% to 400% under 75% RH. The prestretched wet fibers were then hygroscopically equilibrated at 65% RH for 6 h to promote molecular chain alignment and hydrogen bond reorganization, yielding PANa-PAM fibers with distinct uniaxial orientation and crystallinity structures.

Data availability

The data generated in this study are provided in the Supplementary Information/Source Data file. Source data are provided with this paper. Data is available from the corresponding author on request. Source data are provided with this paper.

References

1. Fan, Z. et al. Wearable safeguarding leather composite with excellent sensing, thermal management, and electromagnetic interference shielding. *Adv. Sci.* **10**, 2302412 (2023).
2. Weng, W. et al. A route toward smart system integration: from fiber design to device construction. *Adv. Mater.* **32**, 1902301 (2020).
3. Kanik, M. et al. Strain-programmable fiber-based artificial muscle. *Science* **365**, 145–150 (2019).
4. Liao, X. et al. High strength in combination with high toughness in robust and sustainable polymeric materials. *Science* **366**, 1376–1379 (2019).
5. Xiong, J., Chen, J. & Lee, P. S. Functional fibers and fabrics for soft robotics, wearables, and human-robot interface. *Adv. Mater.* **33**, 2002640 (2021).
6. Jiang, W. et al. Facile fabrication of cotton-based thermoelectric yarns for the construction of textile generator with high performance in human heat harvesting. *Adv. Fiber Mater.* **5**, 1725–1736 (2023).
7. Huang, F.-C., Sun, X.-D., Shi, Y. & Pan, L.-J. Textile electronics for ubiquitous health monitoring. *Soft Sci.* **4**, 40 (2024).
8. Zhu, C., Wu, J., Yan, J. & Liu, X. Advanced fiber materials for wearable electronics. *Adv. Fiber Mater.* **5**, 12–35 (2023).
9. He, W. et al. Establishing superfine nanofibrils for robust polyelectrolyte artificial spider silk and powerful artificial muscles. *Nat. Commun.* **15**, 3485 (2024).
10. Gu, L., Jiang, Y. & Hu, J. Scalable spider-silk-like supertough fibers using a pseudoprotein polymer. *Adv. Mater.* **31**, 1904311 (2019).
11. Li, J. et al. Spider silk-inspired artificial fibers. *Adv. Sci.* **9**, 2103965 (2022).
12. Du, B., Wu, Y., Lu, S., Yang, Z. & Huang, S. Spider-silk-inspired heterogeneous supramolecular network with strain-stiffening, high damping capacity, and supercontraction. *Adv. Funct. Mater.* **33**, 2306071 (2023).
13. Yarger, J. L., Cherry, B. R. & van der Vaart, A. Uncovering the structure-function relationship in spider silk. *Nat. Rev. Mater.* **3**, 18008 (2018).
14. Hou, W., Wang, J. & Lv, J. -a Bioinspired liquid crystalline spinning enables scalable fabrication of high-performing fibrous artificial muscles. *Adv. Mater.* **35**, 2211800 (2023).
15. Du, N. et al. Design of superior spider silk: from nanostructure to mechanical properties. *Biophys. J.* **91**, 4528–4535 (2006).
16. Warwicker, J. O. Comparative studies of fibroins: II. The crystal structures of various fibroins. *J. Mol. Biol.* **2**, 350–362 (1960).
17. Liu, L. et al. Dynamic nanoconfinement enabled highly stretchable and supratough polymeric materials with desirable healability and biocompatibility. *Adv. Mater.* **33**, 2105829 (2021).
18. Kong, Z. et al. Biomimetic ultratough, strong, and ductile artificial polymer fiber based on immovable and slidable cross-links. *Nano Lett.* **23**, 6216–6225 (2023).
19. Wen, K. et al. Jellyfish-inspired artificial spider silk for luminous surgical sutures. *Adv. Mater.* **36**, 2314158 (2024).
20. Shi, Y., Wu, B., Sun, S. & Wu, P. Aqueous spinning of robust, self-healable, and crack-resistant hydrogel microfibers enabled by hydrogen bond nanoconfinement. *Nat. Commun.* **14**, 1370 (2023).
21. Liu, L. et al. Bioinspired strong, tough, and biodegradable poly(vinyl alcohol) and its applications as substrates for humidity sensors. *Adv. Mater. Technol.* **8**, 2201414 (2023).
22. Lang, C. et al. Nanostructured block copolymer muscles. *Nat. Nanotechnol.* **17**, 752–758 (2022).
23. Li, Z. et al. Healable and recyclable elastomers with record-high mechanical robustness, unprecedented crack tolerance, and superhigh elastic restorability. *Adv. Mater.* **33**, 2101498 (2021).
24. Wu, Y. et al. Bioinspired supramolecular fibers drawn from a multiphase self-assembled hydrogel. *Proc. Natl. Acad. Sci.* **114**, 8163–8168 (2017).
25. Wu, Y. et al. Biomimetic supramolecular fibers exhibit water-induced supercontraction. *Adv. Mater.* **30**, 1707169 (2018).
26. Xi, P. et al. Strategy to fabricate a strong and supertough bio-inspired fiber with organic-inorganic networks in a green and scalable way. *ACS Nano* **15**, 16478–16487 (2021).
27. Yu, Y. et al. Biomimetic mineralized organic-inorganic hybrid macrofiber with spider silk-like supertoughness. *Adv. Funct. Mater.* **30**, 1908556 (2020).
28. Bao, B. et al. Rapid fabrication of physically robust hydrogels. *Nat. Mater.* **22**, 1253–1260 (2023).
29. Xiao, Y. et al. Strong and tough biofibers designed by dual cross-linking for sutures. *Adv. Funct. Mater.* **34**, 2313131 (2024).
30. Dou, Y. et al. Artificial spider silk from ion-doped and twisted core-sheath hydrogel fibres. *Nat. Commun.* **10**, 5293 (2019).
31. Mittal, N. et al. Multiscale control of nanocellulose assembly: transferring remarkable nanoscale fibril mechanics to macroscale fibers. *ACS Nano* **12**, 6378–6388 (2018).
32. Wang, X.-Q. et al. Macromolecule conformational shaping for extreme mechanical programming of polymorphic hydrogel fibers. *Nat. Commun.* **13**, 3369 (2022).
33. Wu, S. et al. Spider-silk-inspired strong and tough hydrogel fibers with anti-freezing and water retention properties. *Nat. Commun.* **15**, 4441 (2024).
34. Wang, X.-Q. et al. Structuring and shaping of mechanically robust and functional hydrogels toward wearable and implantable applications. *Adv. Mater.* **36**, 2309952 (2024).
35. Abd Manan, T. et al. Physicochemical properties of absorbent hydrogel polymers in disposable baby diapers. *Chem. Phys. Lett.* **774**, 138605 (2021).
36. Ma, J. et al. Drinking water treatment by stepwise flocculation using polysilicate aluminum magnesium and cationic polyacrylamide. *J. Environ. Chem. Eng.* **7**, 103049 (2019).
37. Ling, S. et al. Polymorphic regenerated silk fibers assembled through bioinspired spinning. *Nat. Commun.* **8**, 1387 (2017).
38. Fang, Y. et al. Toughening hydrogels with fibrillar connected double networks. *Adv. Mater.* **36**, 2822024 (2024).

39. Yang, Y., Ru, Y., Zhao, T. & Liu, M. Bioinspired multiphase composite gel materials: From controlled micro-phase separation to multiple functionalities. *Chem* **9**, 3113–3137 (2023).
40. Koshiro, S. et al. Phase-separation-induced anomalous stiffening, toughening, and self-healing of polyacrylamide gels. *Adv. Mater.* **27**, 26425825 (2015).
41. Ling, S., Kaplan, D. L. & Buehler, M. J. Nanofibrils in nature and materials engineering. *Nat. Rev. Mater.* **3**, 18016 (2018).
42. Gibson, L. J. The hierarchical structure and mechanics of plant materials. *J. R. Soc. Interface* **9**, 2749–2766 (2012).
43. Sørensen, B. E. A revised Michel-Lévy interference colour chart based on first-principles calculations. *Eur. J. Mineral.* **25**, 5–10 (2012).
44. Higgs, M. A. & Sass, R. L. The crystal structure of acrylic acid. *Acta Cryst.* **16**, 657–661 (1963).
45. Liang, J. et al. Bioinspired mechanically robust and recyclable hydrogel microfibers based on hydrogen-bond nanoclusters. *Adv. Sci.* **11**, 2401278 (2024).
46. Kimm, H. J. et al. Rapid fabrication of tendon-inspired ultrastrong, water-rich hydrogel fibers: synergistic engineering of cyano-p-aramid nanofibers and poly(vinyl alcohol). *ACS Nano* **19**, 8316–8327 (2025).
47. Yazawa, K., Malay, A. D., Masunaga, H., Norma-Rashid, Y. & Numata, K. Simultaneous effect of strain rate and humidity on the structure and mechanical behavior of spider silk. *Commun. Mater.* **1**, 10 (2020).
48. Kelly, S. P., Sensenig, A., Lorentz, K. A. & Blackledge, T. A. Damping capacity is evolutionarily conserved in the radial silk of orb-weaving spiders. *Zoology* **114**, 233–238 (2011).
49. Liu, Y., Shao, Z. & Vollrath, F. Relationships between super-contraction and mechanical properties of spider silk. *Nat. Mater.* **4**, 901–905 (2005).
50. Cohen, N., Levin, M. & Eisenbach, C. D. On the origin of super-contraction in spider silk. *Biomacromolecules* **22**, 993–1000 (2021).
51. Madden, J. D. W. et al. Artificial muscle technology: physical principles and naval prospects. *IEEE J. Ocean. Eng.* **29**, 706–728 (2004).

Acknowledgements

This work was supported by the National Natural Science Foundation of China (52303321 to X.Q.W.), the National Natural Science Foundation of Jiangsu Province, China (BK20230501 to X.Q.W.), the Natural Science Foundation of the Jiangsu Higher Education Institutions of China (23KJA430012 to X.Q.W.), the Leading Talents of Innovation and Entrepreneurship of Gusu (ZXL2024370 to X.Q.W.), the China Postdoctoral Science Foundation (Grant Nos. 2024T170632, 2024M752348 to X.Q.W.), Jiangsu Province Young Scientific and Technological Talents Promotion Plan (JSTJ-2024-046 to X.Q.W.), the Opening Project of the Key Laboratory of Bionic Engineering (Ministry of Education), Jilin University (KF2023002 to X.Q.W.). The authors are grateful for the technical support for Nano-X from the Suzhou Institute of Nano-Tech and Nano-Bionics, Chinese Academy of Sciences.

Author contributions

X.Q.W. proposed the research direction and supervised the project. J.Y. and C.C. carried out most experiments and analyzed the data. Y.W. contributed to the structural characterization and analysis of the composite hydrogel fibers. X.P. and G.W.H. contributed to the analysis of nanocrystal structures within composite hydrogel fibers. Q.Z. conducted the WAXS/SAXS characterizations and analysis. L.Y. and S.N. contributed to data analysis. X.Q.W. and J.Y. wrote and revised the manuscript. All authors participated in the discussion and reviewed the manuscript before submission.

Competing interests

The authors declare no competing interests.

Additional information

Supplementary information The online version contains supplementary material available at https://doi.org/10.1038/s41467-025-66537-7.

Correspondence and requests for materials should be addressed to Xiao-Qiao Wang.

Peer review information *Nature Communications* thanks Hang Zhang and the other, anonymous, reviewers for their contribution to the peer review of this work. A peer review file is available.